Autonomic Recovery of Fiber/Matrix Interfacial Bond Strength in a Model Composite

By *Benjamin J. Blaiszik, Marta Baginska, Scott R. White,* and *Nancy R. Sottos**

Autonomic self-healing of interfacial damage in a model single-fiber composite is achieved through sequestration of ca. 1.5 μm diameter dicyclopentadiene (DCPD) healing-agent-filled capsules and recrystallized Grubbs' catalyst to the fiber/matrix interface. When damage initiates at the fiber/matrix interface, the capsules on the fiber surface rupture, and healing agent is released into the crack plane where it contacts the catalyst, initiating polymerization. A protocol for characterizing the efficiency of interfacial healing for the single-fiber system is established. Interfacial shear strength (IFSS), a measure of the bond strength between the fiber and matrix, is evaluated for microbond specimens consisting of a single self-healing functionalized fiber embedded in a microdroplet of epoxy. The initial (virgin) IFSS is equivalent or enhanced by the addition of capsules and catalyst to the interface and up to 44% average recovery of IFSS is achieved in self-healing samples after full interfacial debonding. Examination of the fracture interfaces by scanning electron microscopy reveals further evidence of a polyDCPD film in self-healing samples. Recovery of IFSS is dictated by the bond strength of polyDCPD to the surrounding epoxy matrix.

1. Introduction

Damage in fiber reinforced materials can span multiple lengths scales and is often difficult to detect and repair, leading to expensive maintenance and damage detection requirements. Ideally, a synthetic material should achieve material stasis, such that the original properties are maintained over an extended period of time, even in the presence of damage. In nature, plants and animals achieve material stasis via highly sophisticated autonomic repair and regenerative responses triggered by damage.

Self-healing in synthetic materials has been demonstrated using a variety of methods such as incorporation of healing-agent-filled capsules (capsule-based),[1–15] interconnected vascular networks[16,17] or discrete hollow capillaries,[18–21] or utilizing intrinsic properties of the material.[22–26] Capsule-based self-healing has been demonstrated in bulk thermoset matrices,[1–9] fiber reinforced composite materials[10–14] and elastomers.[15] In these materials, damage triggers the rupture of the embedded capsules, releasing healing agent into the damaged material through capillary action. Polymerization of the healing agent is initiated by contact with an embedded catalyst or secondary polymerizing liquid.

Efforts to develop self-healing fiber-reinforced composites have focused on repair of large- scale delaminations and matrix cracking, but little attention has been given to repair of other composite damage modes. Complex damage modes in fiber-reinforced composites such as matrix cracking, delamination, fiber debonding, and fiber rupture[27,28] present challenges beyond those addressed by self-healing in bulk polymers. In particular, debonding of the reinforcement from the matrix leads to a significant loss of strength and stiffness of the composite by preventing efficient load transfer from fiber to matrix.[29] Additionally, small-scale damage, which may initiate at interfacial defects, can coalesce into large-scale damage during fatigue, ultimately leading to failure of the composite.

Fiber–matrix adhesion is characterized by a variety of testing methods including single-fiber pull-out and microbond,[30–34] single-fiber fragmentation,[35–39] and single-fiber pushout tests.[40–44] Each of these single-fiber tests enables the measurement of the interfacial shear strength (IFSS, τ) between the fiber and matrix. In this work, the single-fiber microbond specimen is adopted for assessing the ability to heal interfacial damage and recover IFSS. Microbond samples consist of a single fiber embedded in a droplet or cylindrical block of matrix material (**Figure 1**) and were prepared in a manner similar to the flat cylindrical specimens described by Zhandarov et al.[30–34] During testing of a microbond specimen, the matrix is constrained and stress is transferred to the matrix-reinforcement interface by pulling on the embedded fiber, which eventually leads to debonding.[30–34]

[*] Prof. N. R. Sottos
Department of Materials Science and Engineering
University of Illinois at Urbana-Champaign
1304 W. Green St., Urbana, IL 61801, USA
E-mail: n-sottos@illinois.edu
Dr. B. J. Blaiszik
Department of Mechanical Science and Engineering
University of Illinois at Urbana-Champaign
IL 61801, USA
M. Baginska, Prof. S. R. White
Department of Aerospace Engineering
University of Illinois at Urbana-Champaign
IL 61801, USA
Prof. S. R. White, Prof. N. R. Sottos
Beckman Institute for Advanced Science and Technology
University of Illinois at Urbana-Champaign
IL 61801, USA

DOI: 10.1002/adfm.201000798

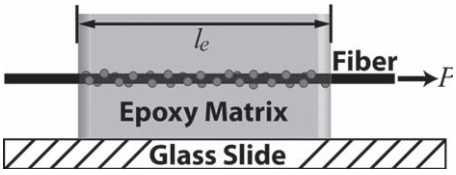

Figure 1. Schematic side view of a microbond specimen with a self-healing functionalized fiber.

Healing of interfacial debonding damage was attempted previously by Sanada et al.[13] using 200 μm diameter DCPD filled microcapsules and Grubbs' catalyst dispersed in a bulk epoxy matrix surrounding a single ca. 14.5 μm glass reinforcing fiber. Sanada et al. achieved healing efficiencies of less than 10% with a 40 wt% loading of microcapsules. Microcapsules of this size scale and weight loading are detrimental to both the fracture toughness and the tensile strength of the epoxy matrix.[2]

In this work, a protocol for healing interfacial damage in fiber-reinforced composite materials is introduced by functionalizing the fiber surface with ca. 1.5 μm diameter healing-agent-filled capsules and catalyst. The effect of this functionalization on the fiber tensile strength and virgin interfacial shear strength is investigated to ensure that the surface treatment does not adversely affect the properties of the fibers or composite system. Self-healing is assessed using a single-fiber microbond test as a model composite (Figure 1). Fiber/matrix interfacial debonding caused by fiber pull-out serves as a trigger to rupture the capsules and deliver healing agent to the damaged region, where it subsequently polymerizes to heal the fiber/matrix interface.

2. Results

2.1. Interfacial Functionalization

Self-healing (SH) fibers were prepared by coating E-glass fibers with Grubbs' catalyst and ca. 1.5 μm diameter capsules containing dicyclopentadiene (DCPD) healing agent. The catalyst and capsules were coated on the glass fibers using two separate dip-coat methods.

For catalyst coating, a 1% solution (wt/wt) of Grubbs' catalyst in benzene was prepared, and a tow of the E-glass fibers (approx. 2000 fibers) was immersed in the catalyst solution for 10–15 s. During this time, the purple catalyst solution was observed to wick into the fiber tow through capillary action. After dipping, the tow was allowed to air dry for 10 min, and was subsequently stored under vacuum to preserve catalyst reactivity. Optionally, the fibers were repeatedly dipped in the catalyst solution to deposit more catalyst.

The amount of catalyst on the surface of the fibers was measured as a mass percent change of the total fiber tow weight, as shown in **Figure 2a**. Catalyst concentration was varied using a higher initial concentration of Grubbs' in benzene, or by repeating the coating process multiple times (Figure 2a). Scanning electron microscopy (SEM) images of the fiber surface, coated with varying catalyst concentrations, are shown in Figure 2b. An optical image of an unfunctionalized glass fiber tow and

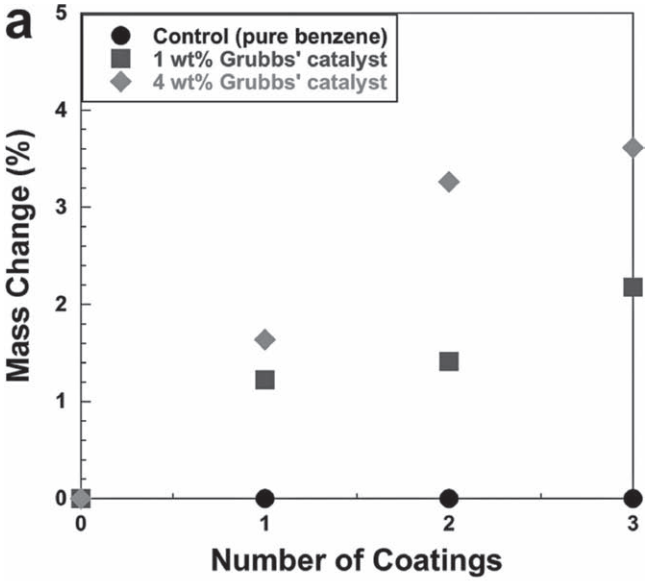

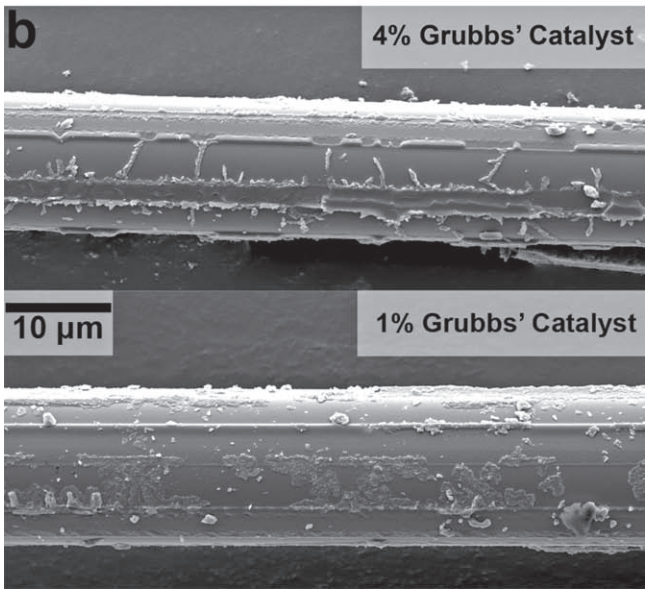

Figure 2. a) Percentage mass change measured for fiber tows dipped in benzene solutions of various concentrations of catalyst. b) SEM micrographs of fibers functionalized with one coating of 4 wt% Grubbs' catalyst solution (top) and 1 wt% Grubbs' catalyst solutions (bottom).

a Grubbs' catalyst functionalized fiber tow is presented in the supporting information (Figure SI1).

After the catalyst was deposited on the fiber tow, the self-healing fibers were then functionalized with DCPD containing microcapsules (ca. 1.5 μm diameter). The capsule area density (ρ) was defined as the total number of capsules per μm^2 of fiber surface area,

$$\rho = \frac{2n}{\pi d L} \quad (1)$$

where d is the measured fiber diameter, L is the measured fiber length and n is the number of capsules visible on the projection

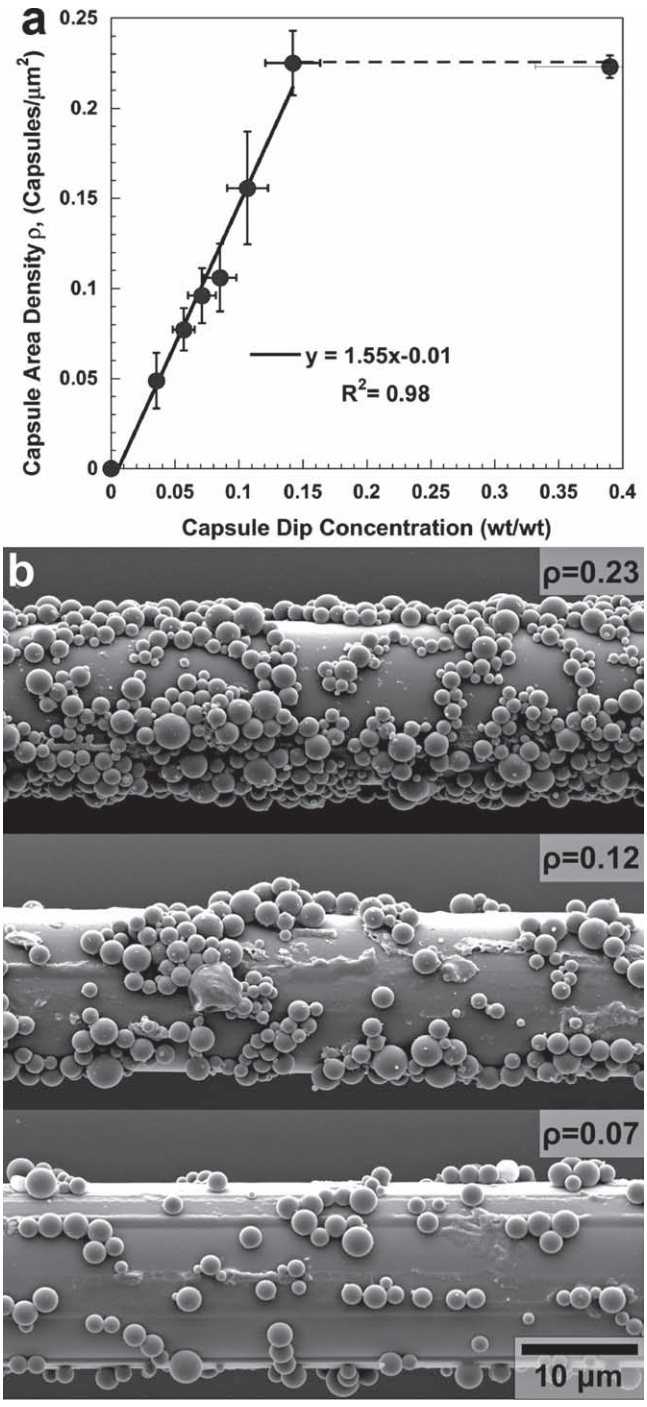

Figure 3. a) Plot showing the correlation between capsule dip concentration and the resulting area density of capsules on the functionalized fiber surface. b) SEM microscopy images of fibers functionalized to various capsule area densities.

of the fiber. As shown in **Figure 3a**, ρ varies linearly with immersion bath concentration to a concentration of 0.15. Above this concentration, the capsule coverage was saturated and a plateau value of $\rho = 0.23$ was achieved (Figure 3a, dashed line). Representative SEM images for capsule area densities ranging from $\rho = 0.05$ to $\rho = 0.23$ are presented in Figure 3b.

Following these catalyst and capsule coating techniques, a series of fiber interfacial functionalizations were selected for the testing described in the following sections. The designation, description, and capsule and catalyst functionalization details for each sample type are provided in **Table 1**.

2.2. Fiber Tensile Strength

The effect of surface treatment on fiber tensile strength was measured for SH functionalized fibers and compared to as received fibers (CI) and fibers functionalized with capsules only (CIII). CI fibers were used as received, CIII fiber controls were exposed to only water during treatment, and the SH fibers were exposed to both benzene and water during functionalization. As shown in **Figure 4**, the strength of the fibers remained approximately 2.0 GPa for all three cases. Hence, functionalization had no effect on the ultimate tensile strength of the fibers.

2.3. Interfacial Shear Strength

Interfacial self-healing was assessed using the microbond test protocol shown schematically in Figure 1, and described in the Experimental section. Optical images of an as received CI fiber microbond specimen and a self-healing SH fiber microbond specimen before testing are presented in **Figure 5**. The CI fiber surface is smooth with few visible imperfections (Figure 5a). In contrast, the SH functionalization is clearly visible on the fiber surface in Figure 5b.

Microbond specimens were tested in a specially designed fixture mounted to a microscope stage. The free end of the fiber was loaded in tension until complete interfacial debonding was achieved and the pull-out force reached a frictional plateau. The specimen was then unloaded, and allowed to heal for 24 h at room temperature before re-testing to measure the recovered interfacial shear stress.

SH specimens and three different types of controls (CI, CII, and CIII), summarized in Table 1, were tested to assess the self-healing and virgin IFSS using the single-fiber microbond method. All samples were identical except for the type of functionalization on the fiber surface. The fibers for the first control specimen group (CI) were as received E-glass fibers. The fibers for the second control specimen group (CII) were functionalized with 1.2% catalyst loading by weight while fibers for the third control group (CIII) were only functionalized with capsules (ρ = 0.12 or ρ = 0.23). Specimens from all control sample groups exhibited no recovery of IFSS. SH samples were functionalized with 1.2% catalyst loading and a variable area density of healing-agent-filled capsules ($\rho = 0.06$–0.23).

Representative virgin and healed load-displacement curves for a SH sample are shown in **Figure 6a**. During initial loading (virgin test – circles), the sample achieved a peak load (P_{Virgin}) of 240 mN before interfacial failure, and then dropped to a frictional plateau of 70 mN. After allowing the sample to heal for 24 h at room temperature, the sample was reloaded (squares) to a peak healed load (P_{Healed}) of 115 mN. The healing efficiency (η) is defined as the ratio of healed and virgin IFSS values,

Table 1. Sample types used to demonstrate interfacial self-healing.

Designation	Description	Capsule Area Density, $\rho\left[\frac{\text{Capsules}}{\mu m^2}\right]$	Grubbs' Catalyst Concentration [Mass Change %]
CI	Control: As received E-glass fiber	–	–
CII	Control: E-glass fiber w/catalyst only	–	1.2
CIII	Control: E-glass fiber w/capsules only	0.23	–
SH(1–3)	Self-healing E-glass fiber w/catalyst and capsules	0.06, 0.12, 0.23	1.2

$$\eta = \frac{\tau_{\text{Healed}}}{\tau_{\text{Virgin}}} = \frac{\left(\frac{P_{\text{Healed}}}{\pi d l_e}\right)}{\left(\frac{P_{\text{Virgin}}}{\pi d l_e}\right)} = \frac{P_{\text{Healed}}}{P_{\text{Virgin}}} \quad (2)$$

For the representative self-healing specimen data shown in Figure 6a, the healed curve exceeds the virgin frictional plateau and achieves a healing efficiency of $\eta = 0.48$. Representative virgin and healed curves for a CI control sample are presented in Figure 6b. When compared to the SH sample in Figure 6a, the curve representing the healed sample only achieves reloading to the frictional plateau value (45 mN), yielding a healing efficiency of $\eta = 0.22$. The frictional plateau load was often higher during the healed test of SH samples, possibly a result of increased interfacial friction as a result of healed material in the crack plane. In contrast, retested control samples often had lower frictional plateau loads, possibly a result of decreased interfacial friction caused by the fiber moving through the sample.

The effect of interfacial functionalization on the virgin fiber/matrix IFSS was investigated for different capsule area densities for SH samples and compared to the controls. The results are summarized in **Figure 7** and **Table 2**. An improvement in the virgin IFSS compared to CI samples was observed for $\rho = 0.06$ and $\rho = 0.12$. For higher capsule density ($\rho = 0.23$), the virgin IFSS decreased to a value similar to the virgin IFSS of the CI specimen group.

The healing efficiency was assessed for each sample group, including controls, and a range of capsule area densities for SH samples (**Figure 8** and Table 2). For control specimens from sample groups CI, CII and CII, the healing efficiencies ranged from $\eta = 0.23$–0.28. The recovery for these controls was only due to the frictional stress associated with pull-out. A low healing efficiency ($\eta = 0.29$) was also measured for SH specimens with low capsule density ($\rho = 0.06$). As the capsule area density increased, the healing efficiency increased significantly when compared to the control samples (see the Supporting Information for additional healed IFSS data). A maximum average healing efficiency of $\eta = 0.44$ was achieved for SH samples with the highest capsule density.

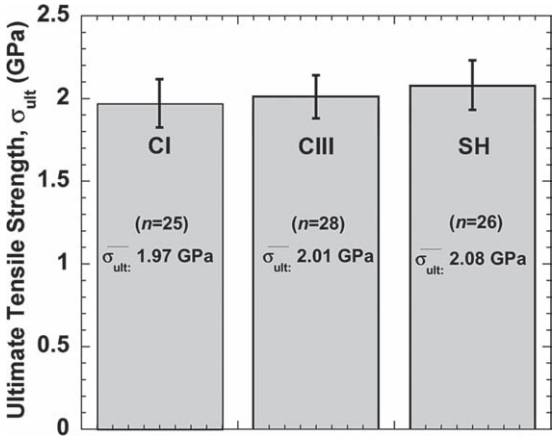

Figure 4. Comparison of tensile strength for as received (CI), capsule functionalized (CIII) and self-healing functionalized (SH) E-glass single fibers. Error bars denote 95% confidence interval and *n* is the number of fibers tested for each sample subset.

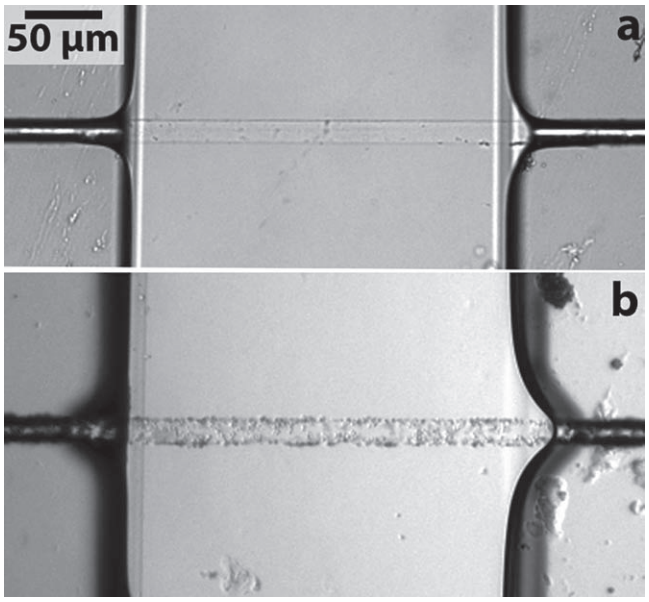

Figure 5. Optical image of (a) CI microbond specimen and (b) SH microbond specimen prior to testing.

2.4. Fractography

The morphology of the healed crack planes in SH and CIII specimens were studied by SEM. Fractography specimens were manufactured using the same protocol as described previously, but the fiber was positioned closer to the top surface to facilitate removal of the fiber after testing. After interfacial debonding, the samples were allowed to heal for 24 h at room temperature. The fiber was removed by pulling vertically to fracture the top surface of the specimen, exposing the interior crack plane morphology for SEM imaging.

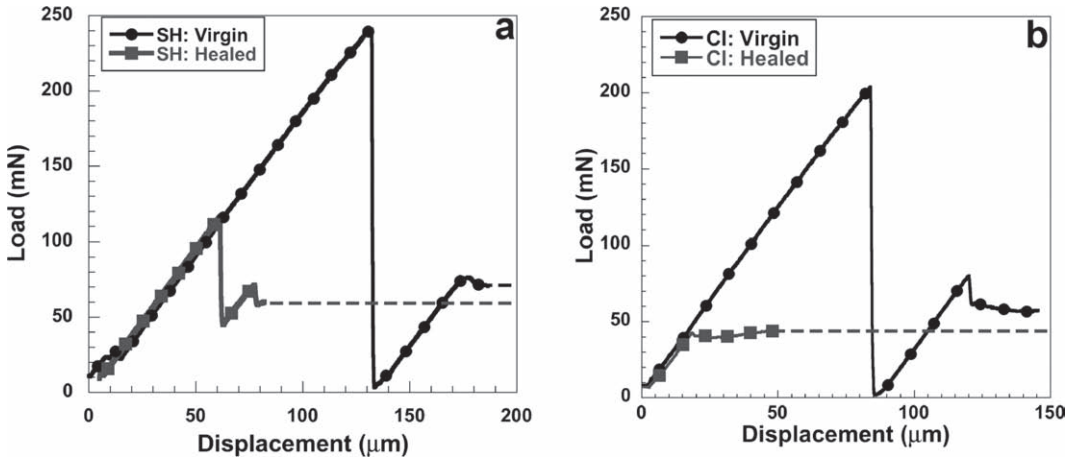

Figure 6. a) Representative virgin (circles) and healed (squares) load-displacement data during pull-out for an SH2 microbond specimen shows IFSS recovery above the virgin frictional plateau. b) Representative virgin (circles) and healed (squares) for CI microbond specimens shows recovery below the frictional plateau.

The interfacial fracture plane of a representative SH sample is shown in **Figure 9a,b**. The fracture plane contains ruptured capsules and evidence of a polyDCPD film. The morphology of the polymer film is rough and contains pores, in great contrast to the smooth surface of the surrounding epoxy. This film is similar to that observed in bulk specimens by Brown et al.[2] The interfacial fracture surface of the CIII control sample is much smoother with ruptured capsules evident in the crack plane, but with no obvious deposition of a healed polymer film (Figure 9c,d).

2.5. Discussion

Self-healing for E-glass fiber and EPON 828/EPIKURE 3274 matrix was achieved with a DCPD-Grubbs' self-healing system. Although DCPD healing agent was used to demonstrate successful interfacial self-healing, the bond strength of DCPD to the glass reinforcement and to the epoxy matrix are not optimal. Addition of coupling agents, development of improved DCPD compatible glass fiber sizings, or the selection of alternate healing-agent monomers will enable increased healing efficiencies in glass fiber-reinforced epoxy composites.

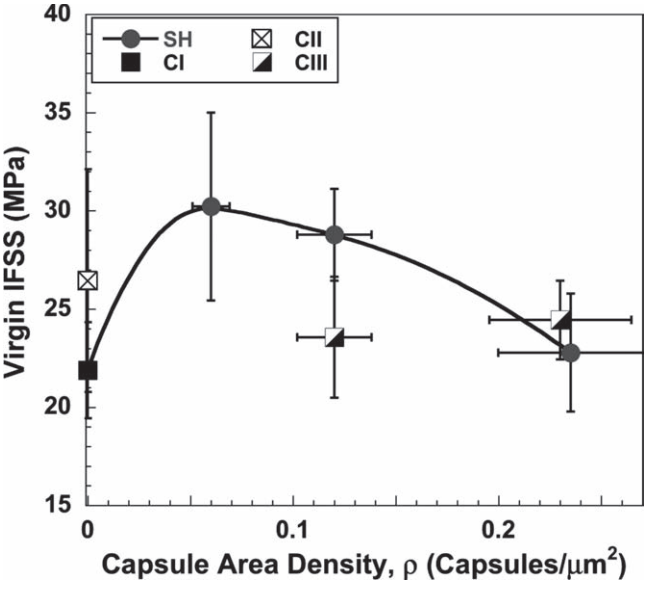

Figure 7. Virgin IFSS for SH fibers, CI as received fiber controls, CII catalyst only controls, and CIII capsule only controls.

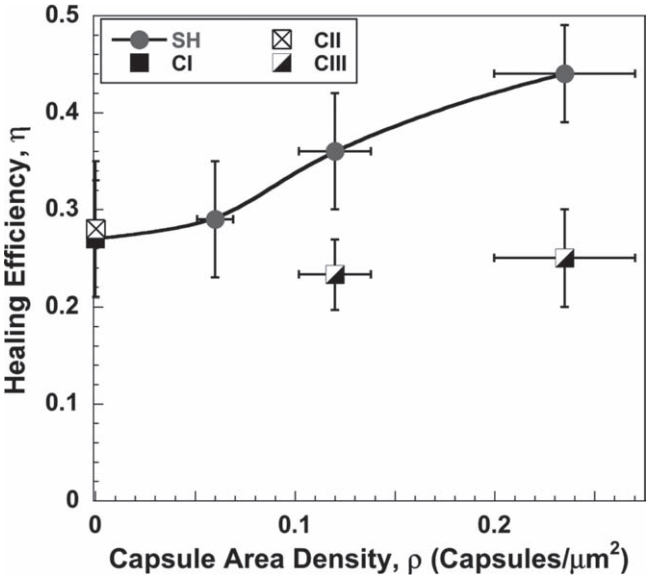

Figure 8. Healing efficiencies for SH fibers, CI as received fiber controls, CII catalyst only controls, and CIII capsule only controls.

In addition to restoration of IFSS, an increase in virgin IFSS was achieved for certain fiber functionalizations. The increased IFSS may be due to the increased surface roughness, evident in Figure 9c,d, provided by the capsules on the fiber. IFSS increases based on the inclusion of fillers at the fiber/matrix interface was reported by Sager et al.[45] Sager et al. reported a 71% increase in IFSS via the addition of carbon nanotubes to the surface of unsized carbon fibers. In the case of interfacial self-healing materials, further studies on the effect of capsule

Table 2. Microbond single-fiber testing results. The error bars indicate the 95% confidence interval of the mean (1.96 standard error).

Sample Designation	Virgin IFSS [MPa]	Healing Efficiency, η	Grubbs' Catalyst Concentration [%]	$\rho[\frac{\text{Capsules}}{\mu m^2}]$
CI: As Received E-Glass Fiber	21.1 ± 2.6	0.23 ± 0.06	0	0
CII: E-glass Fiber w/Catalyst	26.2 ± 5.6	0.28 ± 0.07	1.2	0
CIII: E-glass Fiber w/Capsules	23.3 ± 3.0	0.23 ± 0.04	0	0.12
	23.3 ± 2.4	0.25 ± 0.05	0	0.23
SH1	27.2 ± 4.3	0.29 ± 0.06	1.2	0.06
SH2	25.9 ± 2.1	0.36 ± 0.06	1.2	0.12
SH3	20.5 ± 2.5	0.44 ± 0.05	1.2	0.23

size and the interaction of the capsules with the fiber sizing and the bulk matrix on the IFSS are still required to improve understanding of the observed IFSS increase.

3. Conclusions

Glass fibers were coated with recrystallized Grubbs' catalyst and healing-agent-filled DCPD capsules (ca. 1.5 μm diameter). The tensile strength of the fibers was unaffected by the presence of the self-healing constituents, and the IFSS between the EPON 828/EPIKURE 3274 epoxy and the functionalized fibers was increased by a maximum of 29% for SH specimens when compared to as received glass fiber controls (CI).

Healing of the interfacial bond between E-glass and EPON 828/EPIKURE 3274 was demonstrated using an experimental protocol based on the single-fiber microbond sample, and quantified as the recovery of IFSS. A maximum average healing efficiency of 44% was achieved for SH samples with a high area density of capsules. SEM images of the cylindrical crack plane of SH microbond samples revealed evidence of a polyDCPD polymer film. The ability to heal damage at the fiber/matrix interface before it propagates throughout the matrix may lead to increased damage tolerance and reliability for advanced fiber-reinforced composites.

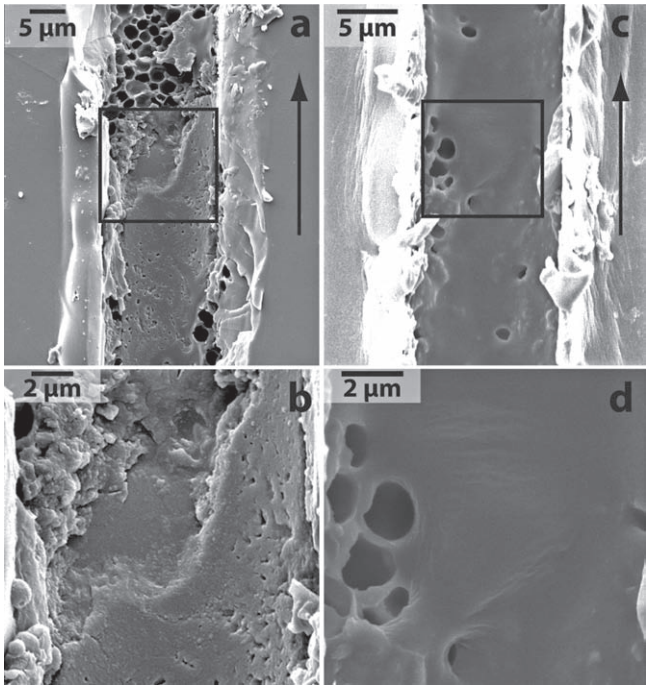

Figure 9. a) SEM image of the interior crack plane of a SH3 microbond specimen functionalized with capsules and catalyst. b) A zoomed image showing the surface morphology of the same SH3 sample. c) SEM image of the interior crack plane of a microbond specimen functionalized with capsules and no catalyst (CIII). d) A zoomed image showing the surface morphology. The arrow represents the direction of force applied to the fiber during pull-out in all images.

Table 3. Properties of fibers used in this study.

Fiber Type	Diameter [μm]	Sizing (Nominal Solids [%])	Ultimate Tensile Strength, σ_{ult} (Gpa)
Owens Corning 158B-AA-675 E-Glass	14.5 ± 0.8	Proprietary epoxy compatible sizing (0.55)	1.97 ± 0.15

4. Experimental Section

4.1. Materials and Methods

Urea, resorcinol, ammonium chloride, formalin (37% formaldehyde), and Grubbs' catalyst powder were purchased from Sigma–Aldrich. The Grubbs' catalyst was recrystallized from benzene (EMD chemicals), prior to use. Dicyclopentadiene (DCPD) was purchased from Acros Organics. ZeMac 400 ethylene-maleic anhydride (EMA, M_w = 400 kDa) copolymer was donated by Vertellus® (formerly Zeeland Chemicals) and used as a 1.25% (wt/vol) aqueous solution. EPON 828 (diglycidyl ether of bisphenol-A) epoxy resin and EPIKURE 3274 curing agent were purchased from Miller-Stephenson. The 750-W Ultrasonic Homogenizer used to prepare the oil emulsion was purchased from Cole-Parmer. Owens Corning 158B-AA-675 E-glass fibers were provided by Owens Corning. Properties for fibers used in this study are presented in **Table 3.**

4.2. Fiber Functionalization Methods

DCPD monomer was encapsulated through in situ polymerization of urea and formaldehyde using the encapsulation procedure described by Blaiszik et al.[46] A 30 mL solution of approximately 1.25% ethylene-maleic

anhydride copolymer (EMA), urea (0.45 g), resorcinol (0.045 g), and ammonium chloride (0.10 g) was stirred for 10 min before adding DCPD (5.45 g). A tapered 3.2-mm tip sonication horn of an ultrasonic homogenizer (750 W) was placed in the solution for 3 min at 40% intensity with continuous mixing at 800 RPM. Next, formalin (1.20 g) was added to the mixing solution to begin polymerization. The temperature control bath was then heated to 55 °C and held constant for 4 h until the reaction was completed. After encapsulation, the capsules were centrifuged and rinsed three times to remove excess surfactant.

DCPD and Grubbs' catalyst test fibers were prepared using a dip-coat technique. Grubbs' catalyst was applied to a fiberglass tow by dipping the tow in a catalyst solution of known concentration, and allowing the catalyst to recrystallize[47] on the glass surface at room temperature (22–23 °C). A single glass fiber from the catalyst coated tow was isolated and dipped once in aqueous DCPD microcapsule solution (approximately 20 mL). The coated fibers were then fixed vertically and allowed to air dry.

4.3. Microbond Specimen Preparation and Testing Method

The microbond sample geometry was prepared by embedding a single glass fiber, optionally coated with self-healing components in an epoxy matrix. The materials required for preparation of microbond samples include epoxy resin and curing agent, glass slides as a substrate for the microbond specimen, EFD syringes, and 100 μm diameter syringe tips. The epoxy was prepared by mixing 100:40 pph EPON 828:EPIKURE 3274, degassing the mixture, and allowing it to react at room temperature for 3 h in a syringe. After 3 h of cure time, the epoxy was sufficiently cured in order to hold its shape after deposition and yet low enough in viscosity to flow through the syringe tip. Single epoxy lines, 200–300 μm wide, were extruded onto glass slides using robotic controlled deposition. Robotic controlled deposition allows the precise three-dimensional placement of extruded material on a substrate.[48] After deposition of the epoxy line, supporting glass fibers were manually placed parallel to the epoxy line to center the fiber in the matrix. Approximately 6.5 h after initial epoxy mixing, the glass fiber to be tested (ca. 1 cm in length) was embedded in the epoxy at the center of the slide, perpendicular to the line of epoxy. After allowing the epoxy to cure 24 h at room temperature and 24 h at 35 °C, cardboard supports were affixed to the slide to prevent premature damage of the fiber/matrix interface.

After curing, samples were loaded into a custom-built load frame and tested under a Leica microscope to observe interfacial debonding as the crack propagated. Optical images were obtained using a Qimaging Micropublisher 3.3 camera. The embedded length (l_e) of individual samples was measured from these images prior to mechanical testing. Samples were loaded in displacement control using a Physik Instrumente M-230.10S linear actuator translating at a rate of 0.5 μm s^{-1} until full interfacial failure. The applied load was measured by a Honeywell Sensotec (150 g) load cell. For a typical sample, the force increased linearly until a debond initiated at the fiber matrix interface near the microbond sample edge closest to the applied load. The force continued to increase as the debond propagated along the interface, in a direction opposite to the applied force, until a peak force (P_{max}) was reached and the fiber completely debonded from the matrix. The load dropped quickly after debonding, but then gradually increased to a plateau value ($P_{Friction}$) dictated by the frictional forces acting on the interface. This generalized behavior was observed for each sample subset in this study (SH, CI, CII, CIII). After the fiber was fully debonded, and the force reached the frictional plateau region, the sample was unloaded and protective cardboard supports were affixed to the specimen and it was allowed to heal for 24 h before testing again.

Interfacial shear strength or IFSS (τ) was calculated from the peak applied load (P_{Max}), the fiber diameter (d), and the embedded length (l_e) as

$$\tau = \frac{P_{Max}}{\pi d l_e} \quad (3)$$

4.4. Tensile Strength Sample Preparation and Testing Method

Fiber tensile strength of the glass fibers was accomplished by first affixing a cardboard cutout to a glass slide with cyanoacrylate glue. Next, a single glass fiber was placed across the cutout, and small droplets of cyanoacrylate glue were used to bond the fiber on both ends. These samples were allowed to cure overnight to ensure the glue was fully polymerized. For tensile testing, a loading rate of 0.083 mm s^{-1} was used following a previous publication by Feih et al.[49] Individual fiber diameters were measured to calculate cross-sectional area and peak stress. Peak ultimate tensile stresses(σ_{ult}) were calculated from the peak load (P_{Max}) and the fiber diameter (d) as

$$\sigma_{ult} = \frac{4 P_{Max}}{\pi d^2} \quad (4)$$

Supporting Information

Supporting Information is available from the Wiley Online Library or from the author.

Acknowledgements

This work was supported by the Air Force Office of Scientific Research (grant no. FA9550-06-1-0553). The authors gratefully acknowledge helpful discussions with Prof. Paul V. Braun, Prof. Phillippe H. Geubelle, Prof. Jeffery S. Moore, Amanda R. Emnett, Andrew R. Hamilton, Amit J. Patel, Jericho L. Moll, David A. McIlroy, and the Autonomic Materials Group at the University of Illinois at Urbana-Champaign. In addition, the authors thank Scott Robinson of the Beckman Imaging Technology Group for assistance with electron microscopy.

Received: April 6, 2010
Revised: May 11, 2010
Published online: August 18, 2010

[1] S. R. White, N. R. Sottos, P. H. Geubelle, J. S. Moore, M. R. Kessler, S. R. Sriram, E. N. Brown, S. Viswanathan, *Nature* **2001**, *409*, 794.
[2] E. N. Brown, N. R. Sottos, S. R. White, *Exp. Mech.* **2002**, *42*, 372.
[3] E. N. Brown, S. R. White, N. R. Sottos, *Compos. Sci. Technol.* **2005**, *65*, 2474.
[4] J. D. Rule, N. R. Sottos, S. R. White, *Polymer* **2007**, *48*, 3520.
[5] M. M. Caruso, B. J. Blaiszik, S. R. White, N. R. Sottos, J. S. Moore, *Adv. Funct. Mater.* **2008**, *18*, 1898.
[6] E. L. Kirkby, J. D. Rule, V. L. Michaud, N. R. Sottos, S. R. White, J. A. E. Manson, *Adv. Funct. Mater.* **2008**, *18*, 2253.
[7] D. S. Xiao, Y. C. Yuan, M. Z. Rong, M. Q. Zhang, *Polymer* **2009**, *50*, 2967.
[8] Y. C. Yuan, M. Z. Rong, M. Q. Zhang, J. Chen, G. C. Yang, X. M. Li, *Macromolecules* **2008**, *41*, 5197.
[9] S. H. Cho, H. M. Andersson, S. R. White, N. R. Sottos, P. V. Braun, *Adv. Mater.* **2006**, *18*, 997.
[10] M. R. Kessler, S. R. White, *Compos. Pt. A – Appl. Sci. Manuf.* **2001**, *32*, 683.
[11] J. L. Moll, S. R. White, N. R. Sottos, *J. Compos. Mater.* **2010**, DOI: 10.177/0021998306356605.
[12] A. J. Patel, N. R. Sottos, E. D. Wetzel, S. R. White, *Compos. Pt. A – Appl. Sci. Manuf.* **2010**, *41*, 360.
[13] K. Sanada, I. Yasuda, Y. Shindo, *Plast. Rubber Compos.* **2006**, *35*, 67.

[14] T. Yin, L. Zhou, M. Z. Rong, M. Q. Zhang, *Smart Mater. Struct.* **2008**, *17*, 015019.
[15] M. W. Keller, S. R. White, N. R. Sottos, *Adv. Funct. Mater* **2007**, *17*, 2399.
[16] K. S. Toohey, N. R. Sottos, J. A. Lewis, J. S. Moore, S. R. White, *Nat. Mater.* **2007**, *6*, 581.
[17] C. J. Hansen, W. Wu, K. S. Toohey, N. R. Sottos, S. R. White, J. A. Lewis, *Adv. Mater.* **2009**, *21*, 4143.
[18] J. W. C. Pang, I. P. Bond, *Compos. Pt. A – Appl. Sci. Manuf.* **2005**, 183.
[19] R. S. Trask, G. J. Williams, I. P. Bond, *J. Royal Soc. Interface* **2007**, *4*, 363.
[20] G. Williams, R. Trask, I. Bond, *Compos. Pt. A – Appl. Sci. Manuf.* **2007**, *38*, 1525.
[21] H. R. Williams, R. S. Trask, I. P. Bond, *Compos. Sci. Technol.* **2008**, *68*, 3171.
[22] X. X. Chen, M. A. Dam, K. Ono, A. Mal, H. B. Shen, S. R. Nutt, K. Sheran, F. Wudl, *Science* **2002**, *295*, 1698.
[23] J. S. Park, K. Takahashi, Z. H. Guo, Y. Wang, E. Bolanos, C. Hamann-Schaffner, E. Murphy, F. Wudl, H. T. Hahn, *J. Compos. Mater.* **2008**, *42*, 2869.
[24] S. J. Kalista, T. C. Ward, *J. R. Soc. Interface* **2007**, *4*, 405.
[25] R. J. Varley, S. Van Der Zwaag, *Acta Mater.* **2008**, *56*, 5737.
[26] P. Cordier, F. Tournilhac, C. Soulie-Ziakovic, L. Leibler, *Nature* **2008**, *451*, 977.
[27] R. Talreja, *Fatigue Fract. Eng. Mater. Struct.* **2006**, *29*, 481.
[28] B. F. Sorensen, R. Talreja, *Int. J. Damage Mech.* **1993**, *2*, 246.
[29] E. E. Gdoutos, K. Pilakoutas, C. A. Rodopoulos, *Failure Analysis of Industrial Composite Materials*, McGraw-Hill, New York, USA **2000**.
[30] S. Zhandarov, E. Pisanova, E. Mader, *J. Adhes. Sci. Technol.* **2005**, *19*, 679.
[31] S. Zhandarov, Y. Gorbatkina, E. Mader, *Compos. Sci. Technol.* **2006**, *66*, 2610.
[32] S. Zhandarov, E. Pisanova, K. Schneider, *J. Adhes. Sci. Technol.* **2000**, *14*, 381.
[33] S. Zhandarov, E. Mader, *J. Adhes. Sci. Technol.* **2005**, *19*, 817.
[34] S. Zhandarov, E. Mader, *J. Adhes. Sci. Technol.* **2003**, *17*, 967.
[35] Y. I. Yilmaz, *J. Compos. Mater.* **2002**, *36*, 537.
[36] H. D. Wagner, J. A. Nairn, M. Detassis, *Appl. Compos. Mater.* **1995**, *2*, 107.
[37] B. W. Kim, J. A. Nairn, *J. Compos. Mater.* **2002**, *36*, 1825.
[38] X. J. Gong, J. A. Arthur, L.S Penn, *Polym. Compos.* **2001**, *22*, 349.
[39] N. J. Wadsworth, I. Spilling, *J. Phys. D: Appl. Phys.* **1968**, *1*, 1058.
[40] G. Lin, P. H. Geubelle, N. R. Sottos, *Int. J. Solids Struct.* **2001**, *38*, 8547.
[41] C. Liang, J. W. Hutchinson, *Mech. Mater.* **1993**, *14*, 207.
[42] R. D. Cordes, I. M. Daniel, *Compos. Eng.* **1995**, *5*, 633.
[43] V. T. Bechel, N. R. Sottos, *J. Mater. Sci.* **1999**, *34*, 3471.
[44] V. T Bechel, N. R. Sottos, *J. Mech. Phys. Solids* **1998**, *46*, 1675.
[45] R. J. Sager, P. J. Klein, D. C. Lagoudas, Q. Zhang, J. Liu, L. Dai, J. W. Baur, *Compos. Sci. Technol.* **2009**, *69*, 898.
[46] B. J. Blaiszik, N. R. Sottos, S. R. White, *Compos. Sci. Technol.* **2008**, *68*, 978.
[47] A. S. Jones, J. D. Rule, J. S. Moore, S. R. White, N. R. Sottos, *Chem. Mater.* **2006**, *18*, 1312.
[48] J. E. Smay, G. M. Gratson, R. F. Shepherd, J. Cesarano, J. A. Lewis, *Adv. Mater.* **2002**, *14*, 1279.
[49] S. Feih, A. Thraner, H. Lilholt, *J. Mater. Sci.* **2005**, *40*, 1615.